scavenging theropods found a few centimeters from the gnawed end of the ischium. Two other broken theropod teeth were found near the shaft of a limb bone. A partial maxilla with teeth may represent another theropod or perhaps another individual of *Cryolophosaurus*.

Non-theropod specimens include a partial articulated left pes of a large prosauropod with the astragalus and metatarsals I through IV (Fig. 3C). This specimen shows the distinctive metatarsal articulation pattern found only in prosauropods (*9*). The distal end of a large prosauropod left femur that was recovered may belong to the same individual. Two articulated, plano-concave cervical vertebrae also appear to be prosauropod. A series of long cervical ribs run parallel to these vertebrae along their ventral side. The preserved portion of the longest of these is 50 cm, and the actual length of the ribs must have been even longer, perhaps as much as 60 cm. Even though these vertebrae were associated with the *Cryolophosaurus* skull, the ribs are several times longer than the cervical ribs of theropods, and the vertebrae lack the pleurocoels that are typical of all theropods.

The collection also contains the humerus of a pterosaur (perhaps dimorphodontid) and a single molar from a large tritylodont. This synapsid is equivalent in size to the largest of the tritylodonts, *Bienotheroides* from the Early Jurassic of China (*10*) and *Tritylodon maximus* from the Early Jurassic of Africa. Thus, the Antarctic fauna from the Falla Formation includes at least six taxa, four of which are dinosaurs.

The age of the fauna is constrained by radiometric and biostratigraphic data. Diabase that is comagmatic with the Kirkpatrick Basalt (177 ± 2 million years ago) (*11*) and intrudes into the upper Falla Formation indicates that the fossils are older than early Middle Jurassic. A *Dicroidium* flora occurs approximately 300 m lower in the section, which constrains the age to Late Triassic or younger (*12*). The fact that prosauropods are restricted to the Late Triassic and Early Jurassic on all of the other continents, along with the considerable stratigraphic distance between *Dicroidium* and the dinosaur locality, suggests that this fauna is most likely Early Jurassic in age. However, because the large prosauropod material appears to be similar to *Plateosaurus* from the latest Triassic, the fauna could conceivably be of that age, although *Cryolophosaurus* is more derived than any of the Triassic theropods.

During the Early Jurassic (Pliensbachian), the approximate paleolatitude of this region of Antarctica could have been as high as 65° to 70° south and was at least 60° (*13*). The large prosauropods and theropods and the pterosaur may have migrated away from harsher winter temperatures; smaller animals such as the tritylodont may have hibernated through a cold season. However, the existence of this fauna suggests that conditions were at least seasonally mild at high latitudes during the early part of the Jurassic.

In addition to the animals found in the Falla Formation, there are tree trunks preserved approximately 4 m above the bones in this section, which indicates the presence of forested areas (*14*). Recent general circulation model (GCM) simulations for the Early Jurassic (*13*) suggest that at high latitudes inland areas experienced climate extremes while coastal areas had milder conditions with seasonal average temperatures never dropping below freezing. Because the Beardmore Glacier region of Antarctica appears to have been near the southern coast of Gondwana during the Jurassic, the existence of this fauna at high latitudes during the Early Jurassic is not in conflict with this model.

REFERENCES AND NOTES

1. E. M. Brouwers *et al.*, *Science* **237**, 1608 (1987).
2. J. J. Hooker, A. C. Milner, S. E. K. Sequeira, *Antarct. Sci.* **3** (No. 3), 331 (1991).
3. P. J. Barrett, D. H. Elliot, J. F. Lindsay, in *Geology of the Central Transantarctic Mountains*, M. D. Turner and J. F. Splettstoesser, Eds. (Antarct. Res. Ser. 36, American Geophysical Union, Washington, DC, 1986), pp. 339–428.
4. The etymology of *Cryolophosaurus ellioti* is as follows: *Cry*, cold in reference to its polar locality; *loph*, crest; *saurus*, lizard; *ellioti*, after D. Elliot, one of the discoverers of the fossil locality. Holotype FMNH PR1821 (Field Museum of Natural History, Chicago, IL).
5. R. E. Molnar, S. M. Kurzanov, Z. Dong, in *The Dinosauria*, D. B. Weishampel, P. Dodson, H. Osmólska, Eds. (Univ. of California Press, Berkeley, CA, 1990), pp. 169–209.
6. J. F. Bonaparte, *Science* **205**, 1377 (1979).
7. T. Rowe and J. Gauthier, in *The Dinosauria*, D. B. Weishampel, P. Dodson, H. Osmólska, Eds. (Univ. of California Press, Berkeley, CA, 1990), pp. 151–168.
8. J. Gauthier, *Calif. Acad. Sci. Mem.* **8** (1986).
9. M. R. Cooper, *Occas. Pap. Natl. Mus. Monum. Rhod. Ser. B Nat. Sci.* **6** (No. 10), 689 (1981).
10. A. Sun, *Sci. Sin.* **27** (No. 9), 970 (1984).
11. A. Heimann, T. H. Fleming, D. H. Elliot, K. A. Foland, *Earth Planet. Sci. Lett.* **111**, 1941 (1994).
12. E. L. Taylor, T. N. Taylor, J. W. Collinson, *Int. J. Coal Geol.* **12**, 657 (1989).
13. M. A. Chandler, D. Rind, R. Ruedy, *Geol. Soc. Am. Bull.* **104**, 543 (1992).
14. Trees are highly carbonized, and ring structures that would indicate the degree of seasonality are not preserved.

15. This work was supported by NSF grants DPP-8817023 and DPP-9118620 to W.R.H. and by the Augustana Research Foundation. We thank D. Elliot and R. Hansen for leading us to the Mount Kirkpatrick site and J. Tamplin, S. Krippner, L. Krissek, and T. Horner for their help in the field. P. Currie, P. Sereno, and M. Parrish offered helpful comments on the material. We also thank M. Parrish and B. Bartels for their suggestions. D. Starenko drafted the full reconstruction of *Cryolophosaurus*.

20 December 1993; accepted 23 March 1994

Diurnal and Semidiurnal Variations in the Earth's Rotation Rate Induced by Oceanic Tides

R. D. Ray, D. J. Steinberg, B. F. Chao, D. E. Cartwright

Recent space-geodetic observations have revealed daily and subdaily variations in the Earth's rotation rate. Although spectral analysis suggests that the variations are primarily of tidal origin, comparisons to previous theoretical predictions based on various ocean models have been less than satisfactory. This disagreement is partly caused by deficiencies in physical modeling. Rotation predictions based on a reliable tidal-height model, with corresponding tidal currents inferred from a modified form of Laplace's momentum equations, yield predictions of tidal variations in Universal Time that agree with very long baseline interferometer observations to 2 microseconds. This agreement resolves a major discrepancy between theory and observation and establishes the dominant role of oceanic tides for inducing variation in the Earth's rotation at these frequencies.

The last several years have witnessed a remarkable development in our ability to monitor high-frequency variations in the Earth's rotation. The observations rely on modern methods of space geodesy: very long baseline interferometry (VLBI), satellite laser ranging (SLR), and the Global Positioning System (GPS). All three measure Earth rotation by determining the three-dimensional orientation of networks of ground observatories relative either to extragalactic radio sources (VLBI) or to the orbital planes of artificial satellites (GPS and SLR). With such technology, special observation campaigns have demonstrated evident daily and subdaily variations in Earth rotation (*1*). In terms of rotation rate, the magnitude of the variations is such that a point on the equator leads and then

R. D. Ray, HSTX, NASA Goddard Space Flight Center, Code 926, Greenbelt, MD 20771, USA.
D. J. Steinberg and B. F. Chao, Geodynamics Branch, NASA Goddard Space Flight Center, Greenbelt, MD 20771, USA.
D. E. Cartwright, Borough House, Petersfield, Hampshire GU32 3LF, United Kingdom.

lags a point on a uniformly rotating Earth by roughly 2 or 3 cm (*2*).

A recent spectral analysis of 8 years of VLBI data by Herring and Dong (*3*) strongly suggests that these daily and subdaily variations in rotation originate with the oceanic tides: These authors observed isolated spectral peaks at the known tidal frequencies. The oceanic tides affect Earth rotation through two mechanisms: changes in the Earth's inertia tensor, which are induced by varying tidal heights, and changes in the relative angular momentum between ocean and mantle, which are induced by varying tidal currents. The second mechanism appears to be more important for short-period tidal variations in the rotation rate (*4*).

Global numerical models of the ocean tides may be used to predict variations in Earth rotation. These models can be separated into two classes: those constrained to reproduce in situ tidal measurements and those unconstrained by any measurements and dependent only on knowledge of the global bathymetry. Previous predictions of tidal variations in Earth rotation (*5, 6*) have been based on unconstrained models. To be successful, such an approach requires sophisticated hydrodynamic modeling, and the results are generally accurate only if fine spatial resolutions are maintained in shelf areas so that important nonlinear mechanisms (for example, quadratic bottom friction and constituent interactions) can be properly modeled (*7*). The shallow seas, after all, have been known for decades as the principal region of tidal energy dissipation, and many numerical experiments have proven the global tide's sensitivity to shelf physics (*8*).

Historically, the most reliable global tide models have been those constrained by observations—typically observations of tidal elevation obtained by gauges along coastlines and at islands and, more recently, by satellite altimetry. Such observations reduce the severe demands for accurate physical modeling that unconstrained methods must meet. We followed this approach by adopting the model of global tidal heights derived by Schwiderski (*9*). This model is known to be fairly reliable because it was constrained by more than 2000 coastal, island, and bottom pressure measurements; its root-mean-square (rms) discrepancy with 80 selected open ocean "ground truth" height measurements is about 4 cm for the principal semidiurnal lunar constituent (*10*).

From the adopted global height fields, we computed tidal currents using Laplace's tidal equations. These current calculations are restricted to the deep ocean. Although currents in shallow seas are typically an order of magnitude greater than currents in the open ocean, the small volume of the shallows (~0.5% of the global ocean) ensures that these regions contribute no more than a few percent to global momentum calculations. This restriction has two benefits: It allows us to invoke dynamical equations appropriate strictly to open ocean conditions, which are considerably

Table 1. The UT1 tidal variations (in microseconds). Each tidal constituent is denoted according to original Kelvin-Darwin naming conventions. Entries list in-phase (Cos) and quadrature (Sin) contributions to ΔUT1 relative to the tidal potential at Greenwich, with each tide broken into components from inertia (height) terms and relative angular momentum (current) terms. Phase convention is consistent with that of Gross (*14*).

Tide	Period (hours)	Heights		Currents	
		Cos	Sin	Cos	Sin
Q_1	26.868	0.86	0.58	3.23	0.72
O_1	25.819	2.67	3.51	13.82	8.56
P_1	24.066	0.93	−1.22	4.66	3.16
K_1	23.935	2.34	−3.49	16.52	13.28
N_2	12.658	0.05	0.21	−1.87	−3.37
M_2	12.421	5.50	−0.37	−13.58	−16.48
S_2	12.000	1.92	2.57	−3.80	−10.01
K_2	11.967	0.57	0.80	−0.90	−2.69

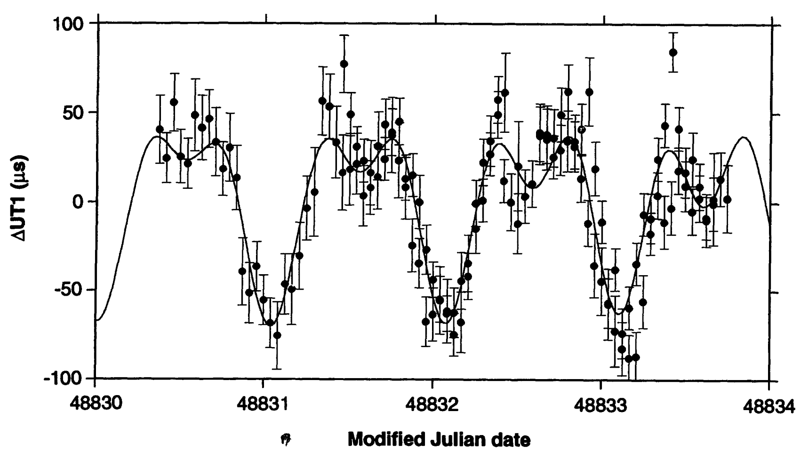

Fig. 1. Predicted and observed variations in ΔUT1. The prediction (solid curve) follows from Eq. 2 with use of our harmonic constants from Table 2. The observations (*18*), with 1σ standard errors, are the product of five overlapping VLBI experiments carried out during late July 1992 (modified Julian date 48830 = 27 July 1992). Each experiment was about 1 day long, and each has been adjusted here empirically by a single bias.

Table 2. Tidal ΔUT1 comparisons of amplitudes (in microseconds) and phase lags (in degrees) relative to equilibrium arguments at the Greenwich meridian. Sovers *et al.* (*15*) and Herring and Dong (*3*) are estimates based on VLBI data; Broche *et al.* (*5*) [which was later modified (*14, 19*)] and this paper are model predictions (*20*).

Study	Diurnal tides				Semidiurnal tides			
	Q_1	O_1	P_1	K_1	N_2	M_2	S_2	K_2
Sovers *et al.*	6.6, 37.0°	21.4, 39.1°	7.2, 26.6°	15.5, 13.0°	3.0, 221.0°	18.2, 235.1°	5.2, 265.6°	2.8, 250.9°
Herring and Dong	5.3, 35.8°	23.6, 47.1°	7.1, 33.5°	18.9, 20.1°	3.2, 240.3°	17.9, 232.9°	8.6, 269.3°	3.8, 257.8°
Brosche *et al.**		35.2, 21.8°	7.1, 59.4°	18.7, 52.0°	7.5, 231.4°	35.3, 229.9°	18.1, 260.0°	
This paper	4.3, 17.6°	20.4, 36.2°	5.9, 19.2°	21.2, 27.4°	3.6, 240.1°	18.7, 244.4°	7.7, 255.8°	1.9, 260.1°

*As amended and tabulated by Gross (*14*).

simpler than equations for shallow water, and it allows us to ignore known errors in the tidal heights in the shelf regions.

Let u (southward) and v (eastward) be complex variables whose real and imaginary components give the barotropic, or depth-averaged, tidal current velocities in phase and in quadrature to the tide-generating potential Φ. Similarly, let ζ be a complex tidal height, reckoned with respect to the seabed. For a constituent of frequency ω, Laplace's tidal equations, modified for the ocean's loading and compression of the solid Earth and for the tide's own gravitational self-attraction, may be written in spherical polar coordinates as

$$i\omega u + fv = \frac{g}{a}\frac{\partial}{\partial\theta}(\zeta - \gamma_2\Phi - \Upsilon)$$

$$i\omega v - fu = \frac{g}{a \sin\theta}\frac{\partial}{\partial\varphi}(\zeta - \gamma_2\Phi - \Upsilon) \quad (1)$$

where g is the gravitational acceleration, a the Earth's mean radius, γ_2 a degree-2 Love number, and f the Coriolis parameter. The quantity Υ modifies the astronomical potential Φ for the ocean loading and self-attraction and is here computed from a spherical harmonic decomposition of ζ to degree and order 180 (*11*). Note that Eq. 1 neglects bottom friction. In the deep ocean, any physically plausible representation of friction is easily shown to be two or three orders of magnitude less than the leading terms in Laplace's equations (the net global effect of friction is nevertheless implied in the known field of ζ).

Because the right side of Eq. 1 is known, current components u and v are easily found, excepting for known singularities at the "critical latitudes" where the inertial and tidal frequencies are equal. Test calculations show that u and v remain stable until within 5° of the critical latitudes, so we simply interpolate across the remaining 10° gap (*12*). More details of these calculations, as well as comparisons to in situ current measurements, may be found in (*13*).

Daily and subdaily variations in the Earth's rotation rate are conveniently parameterized by the quantity ΔUT1, representing the departure of Universal Time UT1, as regulated by the Earth's rotation, from atomic time TAI. The perturbations in ΔUT1 that are induced by oceanic tides follow from equation 6 of Gross (*14*) and consist of two terms: one dependent on the axial component of relative angular momentum, which we compute from our tidal currents, and a second dependent on the axial moment of inertia, which we compute from the second-degree zonal harmonic of the tidal heights (neglecting a small zero-degree harmonic arising from nonconservation of mass). The second term contains factors allowing for ocean loading, and both terms allow for fluid-core decoupling. The resulting ΔUT1 variations for the eight major diurnal and semidiurnal tides (Table 1) and comparison of the totals with other results (Table 2) show that three tidal constituents clearly dominate ΔUT1: M_2, O_1, and K_1.

Table 2 shows generally good agreement between our constants and the observed values. In terms of sine and cosine components, the rms difference with the estimates of Herring and Dong (*3*) is 2.1 μs and with those of Sovers *et al.* (*15*) is 2.2 μs. These VLBI estimates themselves differ by 1.8 μs rms, whereas the difference between Sovers *et al.* and Brosche *et al.* (*5*), a model prediction, is 8.7 μs. Discrepancies of 2 μs are comparable with the quoted standard errors of Sovers *et al.* Part of the remaining discrepancies in diurnal tides may be attributable to our approximations near the critical latitudes (which occur between 25° and 30°; in contrast, all semidiurnal tides have critical latitudes in the Arctic, where errors should have little influence on UT1). Other discrepancies in the lunar tides may be attributable to an apparent lack of nodal corrections in the VLBI analyses; for observations taken in the late 1980s, nodal corrections are especially important for K_2 and O_1, and they would reduce the reported observed amplitudes.

The harmonic constants in Table 2 may be used to predict ΔUT1 at any time t according to

$$\Delta\mathrm{UT1} = \sum_{i=1}^{8} H_i f_i \cos(\chi_i + u_i - G_i) \quad (2)$$

where χ_i represents the classical Doodson arguments for each tide evaluated at t, H_i and G_i are amplitudes and Greenwich phase lags, respectively, as given in Table 2, and f_i and u_i account for nodal modulations in lunar constituents (*16*).

The convergence of observation and theory (Table 2 and Fig. 1) is remarkably good and clearly establishes the primary role of the oceans in inducing these Earth rotation variations. Earth libration (*17*) and atmospheric tides must also induce ΔUT1 variations, but these are secondary effects and will require improved precision before they are detected. The observational determinations will certainly improve as space geodetic measurements continue to accumulate. Within the next few years, tide models based on the TOPEX (Ocean Topography Experiment) Poseidon satellite altimeter mission will appear; their Earth rotation predictions should be more accurate than present models, especially when derived through data-assimilation schemes.

REFERENCES AND NOTES

1. S. M. Lichten, S. L. Marcus, J. O. Dickey, *Geophys. Res. Lett.* **19**, 537 (1992).
2. Variations in the orientation of the rotation axis (polar motion) have also been detected and are of great interest, but polar motion is fraught with a number of technical subtleties that we prefer to discuss at length elsewhere.
3. T. A. Herring and D. Dong, *J. Geophys. Res.*, in press.
4. H.-R. Baader, P. Brosche, W. Hövel, *Z. Geophys.* **52**, 140 (1983).
5. P. Brosche, U. Seiler, J. Sündermann, J. Wünsch, *Astron. Astrophys.* **220**, 318 (1989); U. Seiler, *J. Geophys. Res.* **96**, 10287 (1991).
6. S. R. Dickman, *Geophys. J. Int.* **112**, 448 (1993).
7. C. Le Provost, G. Rougier, A. Poncet, *J. Phys. Oceanogr.* **11**, 1123 (1981); P. Vincent and C. Le Provost, *J. Geophys. Res.* **93**, 543 (1988).
8. G. I. Marchuk and B. A. Kagan, *Dynamics of Ocean Tides* (Kluwer Academic, Dordrecht, Netherlands, 1989).
9. E. W. Schwiderski, *Rev. Geophys. Space Phys.* **18**, 243 (1980).
10. R. D. Ray, *IEEE Trans. Geosci. Remote Sensing* **31**, 355 (1993). Although the altimeter-derived model of D. E. Cartwright and R. D. Ray [*J. Geophys. Res.* **95**, 3069 (1990)] may be slightly more accurate than the Schwiderski model, particularly for the principal M_2 tide, it is spatially noisier (because it is a strictly empirical model), making its use in the Laplace equations problematic because the required spatial derivatives tend to enhance noise. See (*13*).
11. M. C. Hendershott, *Geophys. J. R. Astron. Soc.* **29**, 389 (1972); R. D. Ray and B. V. Sanchez, *NASA Tech. Memo. 100743* (1989).
12. If u and v are transformed into cyclonic and anticyclonic components $r^+ = ½(u - iv)$ and $r^- = ½(u^* - iv^*)$, respectively (for the northern hemisphere), it may be shown that only the anticyclonic components are singular at the critical latitudes, and thus, only they require interpolation; the cyclonic components may be evaluated directly without modification.
13. D. E. Cartwright, R. D. Ray, B. V. Sanchez, *NASA Tech. Memo. 104578* (1992).
14. R. S. Gross, *Geophys. Res. Lett.* **20**, 293 (1993).
15. O. J. Sovers, C. S. Jacobs, R. S. Gross, *J. Geophys. Res.* **98**, 19959 (1993).
16. A. T. Doodson and H. D. Warburg, *Admiralty Manual of Tides* (Her Majesty's Stationary Office, London, 1941). This standard use of f_i and u_i may be more problematic for polar motion, with its resonance near K_1, but there should be no such difficulties for UT1, at least at present levels of uncertainties.
17. B. F. Chao, D. N. Dong, H. S. Liu, T. A. Herring, *Geophys. Res. Lett.* **18**, 2007 (1991).
18. Observations for Fig. 1 were provided by J. Gipson and C. Ma (unpublished data) of the VLBI group at NASA Goddard Space Flight Center.
19. J. Wünsch and J. Busshoff, *Astron. Astrophys.* **266**, 588 (1992).
20. M. M. Watkins and R. J. Eanes [in *Geodesy and Physics of the Earth*, H. Montag and C. Reigber, Eds. (Springer-Verlag, Berlin, 1993), pp. 400–403] used SLR data and reported amplitude and phase-lag estimates for two tides: O_1 (26 μs, 52°) and M_2 (18 μs, 248°). Herring and Dong (*3*) also estimated M_2 from what is apparently the only extant dataset of currents computed by Schwiderski; they got 18.1 μs and 249.2°, in close agreement with our entry in Table 2, as well as with the VLBI and SLR values.

21. Supported in part by the Geophysics Program of the National Aeronautics and Space Administration.

27 December 1993; accepted 25 March 1994